IIETA International Information and Engineering Technology Association
Advancing the World of Information and Engineering

Traitement du Signal
Vol. 42, No. 6, December, 2025, pp. 3555-3571
Journal homepage: http://iieta.org/journals/ts

# Efficient Recurrent Forcing Fourier Phase Distortionless Response Network for Modern Mobile Networks

Bhagyashri Warhade*, Rupali Patil

G H Raisoni College of Engineering and Management, Savitribai Phule Pune University, Pune 412207, India

Corresponding Author Email: bhagyashri.warhade@gmail.com



https://doi.org/10.18280/ts.420639

**Received:** 17 March 2025
**Revised:** 10 June 2025
**Accepted:** 28 July 2025
**Available online:** 31 December 2025

***Keywords:***
*beamforming, millimeter wave, massive MIMO, mobile networks, CTI, ISI*

**ABSTRACT**

Multi-user millimeter-wave (mmWave) massive MIMO systems are essential for next-generation wireless networks, offering broad bandwidth and elevated data transmission rates. However, the existing methods face challenges such as signal scattering, interference, and cross-technology noise. To overcome these challenges, a novel Recurrent Butler Forcing Attenuators Fourier phase Distortionless Response Network is proposed to improve beamforming accuracy and performance of the system. Moreover, multi-path fading in advanced beamforming causes Inter-Symbol Interference (ISI), where delayed signals overlap and lead to decoding errors. To address this, the first Recurrent Neural Network (RNN) layer uses an Amalgam Butler Zero Forcing Matrix. This optimized beamforming matrix, combined with zero-forcing algorithms, mitigates out-of-phase signals and improves demodulation accuracy. In the second RNN layer, Debauched Attenuators Fourier Transform (DAFT) dynamically adjusts signal amplitudes using attenuators and applies Fast Fourier Transform (FFT) for frequency analysis. This enhances the system's ability to detect and mitigate interference. Further, the presence of multiple wireless technologies in the same environment introduces cross-technology interference (CTI), disrupting beamforming accuracy. To combat this, the Phase Tiniest Variance Signal Response (PTVSR) strategy is developed, which is integrated into the third layer of the RNN, it dynamically adjusts signal phases and optimally combines signals using the Minimum Variance Distortionless Response (MVDR) algorithm. This approach reduces CTI-induced errors and creates more accurate beam patterns in complex environments. As a result, the proposed model outperforms existing methods, achieving higher accuracy, spectral efficiency, and sum rate.

## 1. INTRODUCTION

The backbone of today's communication systems is made up of mobile networks, sometimes referred to as cellular networks, which provide voice and data services on portable electronics, including smartphones and tablets. Through several generations, each characterized by advancements in technology and capacities, these networks have undergone substantial evolution throughout time. Massive MIMO beamforming is essential for improving performance in modern mobile networks. By using a wide range of antennas at the base station, these methods may connect with several users at once and make use of spatial diversity to boost spectral efficiency and signal quality. Popular beamforming techniques include maximum ratio transmission and zero-forcing, which seek to maximize signal power and eliminate interference, respectively. However, massive MIMO faces challenges like hardware complexity and energy use, which demand advanced signal processing. Other key challenges are the need for accurate channel data and the effect of user mobility on beamforming performance. To fully reap the benefits of massive MIMO and facilitate the future rollout of dependable and efficient mobile communication systems, these obstacles need to be overcome [1-4].

While the transmitter generates a signal, the surroundings contain barriers such as buildings and trees, causing the signal to bounce around and follow multiple pathways before reaching the receiver. This bouncing about is known as multi-path fading, and it results in Inter-Symbol Interference (ISI). Various approaches are used to precisely demodulate and recover original symbols in the presence of ISI. Equalization methods, such as linear equalizers and decision feedback equalizers, are widely used to reduce ISI effects by altering the incoming signal. Another technique is the maximum likelihood sequence estimate, which searches for the most probable broadcast sequence based on the received signal. Furthermore, filter settings are continually adjusted using adaptive equalization algorithms in response to shifting channel circumstances. Notwithstanding these techniques, problems still exist, such as the requirement for precise channel status data, sensitivity to noise and interference, and the difficulty of putting adaptive algorithms into practice. Moreover, obtaining the best demodulation and symbol recovery can be severely hampered by time-varying features and non-linearities in the communication channel. Improving communication system performance in the context of multi-path fading and ISI continues to be a focus of developing reliable and computationally efficient solutions to solve these

issues [5-8].

Another component that has to be considered to further enhance the quality of signal transmission is angular resolution, since it is necessary to minimize undesired signal transmission in other directions. The capacity to discern between sources that are closely spaced in the angular domain is referred to as angular resolution in beamforming. An array of sensors with separated components is a popular way to acquire angular resolution. Spatial diversity is used to differentiate between incoming signals originating from various directions. A different strategy is to use shorter wavelengths or higher frequencies, which by definition have a smaller beam width and hence offer superior angular resolution. Nevertheless, actual implementations face difficulties, such as the requirement for higher hardware costs and computational complexity when using dense sensor arrays. In addition, angular resolution can be deteriorated by problems such as multipath propagation, mistakes in data processing, and mutual coupling between sensors. In beamforming applications, finding the ideal angular resolution continues to be a constant problem of balancing system complexity and performance [9-12].

Additionally, to the aforementioned factors, another dynamic aspect that affects the effective transmission of signals across diverse wirelessly connected devices is cross-technology interference (CTI). When signals from many technologies interfere with one another, particularly in the millimeter-wave (mmWave) band, this phenomenon is referred to as CTI. Several techniques are used to reduce CTI in mmWave communications. To concentrate signals and lessen interference, one method uses sophisticated signal processing techniques like beamforming and beam steering. Using sophisticated coding and modulation techniques to increase signal resilience in the face of interference is another tactic. Furthermore, approaches for allocating resources in the frequency and temporal domains are utilized to maximize the utilization of available spectrum and reduce interference. Nevertheless, there are drawbacks to these techniques, such as higher computing complexity, power consumption, and the requirement for complicated gear. Moreover, the dynamic character of wireless environments and the cohabitation of many technologies present continuous difficulties in the development of adaptive and successful CTI mitigation techniques for mmWave communication networks. To fully utilize mmWave technology in the future wireless communication networks, these issues need to be resolved [13-15].

Despite significant progress in improving the efficiency and simplifying multi-user mmWave massive MIMO systems, numerous enhancements are still needed to achieve a better propagation path through efficient angular resolution, avoiding inference, and other research limitations.

### 1.1 Main contribution of this study

The following methodological and experimental contributions have been achieved by this paper:

• To overcome overlapping symbols and decoding problems due to ISI, an Amalgam Butler Zero Forcing Matrix in the RNN's first layer is introduced, in which Butler matrix optimizes beamforming and zero-forcing algorithms to minimize ISI and mitigate, thereby enhancing signal demodulation in heavily scattered environments.

• To effectively handle varying angular resolutions, DAFT is introduced in RNN's second layer. In which attenuators dynamically adjust signal amplitudes and FFT performs frequency-domain analysis, ensuring consistent performance in mmWave communication systems amidst interference.

• To mitigate the CTI from coexisting wireless technologies, the Phase Tiniest Variance Signal Response (PTVSR) is utilized in RNN's third layer. This combines phase shifters and the MVDR algorithm to suppress noise and enhance beamforming accuracy, resulting in precise beamforming and improved performance in environments with diverse wireless technologies.

### 1.2 Organization of the paper

This work is divided into the following sections. Section 2 discusses the existing literature on mmWave communication systems and summarizes the available approaches. Section 3 explains the suggested approach and workflow for this work. Section 4 explains the datasets, as well as the experimental methodology, the analytical results, and the comparison to previous investigations. Finally, Section 5 sums up the study.

## 2. LITERATURE SURVEY

This literature review examines existing research efforts focused on improving the performance of large MIMO systems, given the complexity and quick improvements in mmWave communication systems. To overcome issues like inter-user interference, hybrid beamforming, and computational complexity, the study explores creative solutions put forth by different researchers. This provides an understanding of how mmWave communication technologies are developing.

Carrera et al. [16] examined the concept of improving multi-user millimeter wave (mmWave) communications performance in three stages. The first is achieved by applying a revised pilot mapping to minimize inter-user interference and achieve more precise channel estimations. The second step involved designing a hybrid receiver that, depending on the accuracy of the Channel State Information (CSI), selected between the multi-user regularized zero-forcing beamforming (RZFBF) and the minimum mean square error (MMSE) receivers to combine/precode the massive multiple-input multiple-output (MIMO) signal. To enhance multi-user efficiency and lessen inter-user interference, it was suggested that, during the third phase of uplink communications, the beam direction be enhanced with a little change in azimuth angle. However, this kind of structure's computational complexity and hardware design are now too costly for widespread use.

Dilli [17] developed a downlink hybrid beamforming communication system for multiple users that was multi-user mMIMO and had several independent data streams per user as well as accurate channel status information. It focused on the mmWave MU-mIMO hybrid beamforming system's hybrid precoding at the transmitter and combining at the receiver. The study's conclusions illustrate the trade-off between the number of BS antennas required and the number of data streams per user. To achieve higher order throughputs in mmWave MU-mMIMO systems, it was highly suggested to employ more parallel data streams per user. On the other hand, more data streams per user result in increased interference and possible user crosstalk.

Zhang et al. [18] examined a multiuser, sub-connected, mmWave large MIMO system with a hybrid (analog/digital) beamforming architecture. Focus on this system's sum-rate maximization problem. The receiver and transmitter were jointly designed using a two-stage design method. The proposed piecewise dual joint iterative approximation (PDJIA) approach was used to construct the analogue beamformer and combiner. This method provided both closed-form solutions and linear properties. By using the baseband piecewise successive approximation approach, the problem of digital beamforming was addressed and the number of consumers serviced can be efficiently increased. Furthermore, the proposed techniques result in sensitivity to changes in the channel conditions.

Huang et al. [19] presented a framework for extreme learning machines (ELMs) to simultaneously optimize beamformers for transmission and reception. Initially, describe an HBF approach based on fractional programming and majorization-minimization to provide precise labels for training. Then, to increase beamformer resilience, an ELM-based HBF (ELM-HBF) design was offered. In comparison to traditional methods, higher system sum rates were achieved with both FP-MM-HBF and ELM-HBF. Moreover, ELM-HBF required incredibly little time to calculate and had good HBF performance. It is necessary to evaluate the proposed framework's scalability to bigger and more intricate communication networks.

Zhang et al. [20] focused on the full-connected topology-based hybrid beamforming design of a downlink mmWave massive multi-user MIMO (MU-MIMO) system, with the target function of system sum rate optimization. In the piecewise successive iterative approximation (PSIA) technique, the analogue beamformer and combiner were constructed during the analogue beamforming step. This approach produced closed-form answers in addition to its linear characteristic. The piecewise successive approximation approach, which was simple to implement and helped reduce computation complexity, was used in the digital beamforming stage to design the digital beamforming based on the necessity to prevent information loss. However, the massive MIMO systems are designed to handle a large number of antennas, so the scalability of the PSIA approach should be carefully evaluated.

Zhang et al. [21] investigated the hybrid beamforming technique for the big MIMO relay system with mixed and full-connected structures in the decode-and-forward (DF) milliwave. Maximize the aggregate rate of the entire system to optimize hybrid beamforming in relay systems as an objective function. Then, to minimize computing complexity, reformulate the original problem into two single-hop mmWave MIMO sum-rate maximization sub problems. The piecewise successive approximation technique is then provided, based on the criterion that simultaneously designs the analogue and digital beamforming stages while trying to prevent information loss at each level. Nevertheless, there are difficulties in reaching convergence using the sequential approximation approach since it requires repeated optimization at every level.

Lizarraga et al. [22] proposed a hybrid beamforming technique for a multiuser huge MIMO system that is based on deep reinforcement learning (DRL). This approach allows the analogue beamforming matrix to be updated iteratively while scheduling individual users. In addition to this approach, a Singular Value Decomposition operation in a reduced-size channel matrix was employed to determine the hybrid beamforming scheme's most practical digital precoder matrix. The DRL processing was centralized in the receiver to service the scheduled user. It used a low-rate feedback channel to determine the most useful update of the analogue beamforming matrix coefficient. It is necessary to evaluate the proposed framework's scalability to bigger and more intricate communication networks.

Jafri et al. [23] designed a hybrid beamformer for a multi-user multi-cell (MUMC) mmWave system that utilized transmit power reduction and BS coordination, subject to realistic limitations on the signal-to-interference-plus-noise ratio (SINR) at each mobile station. In the beginning, a centralized MUMC system's completely digital beamformer with flawless CSI was identified using a semidefinite relaxation-based method. Next, the fully-digital (FD) solution was divided into its analogue and digital components using a Bayesian learning approach to build a hybrid transceiver. To eliminate the substantial signalling overheads required by the centralized approach, a distributed hybrid beamformer based on the alternating direction method of multipliers was devised for the same system. This beamformer only required local CSI and minimal information transmission across the BSs. In dynamic situations, the performance of coordinated hybrid beamforming solutions for MUMC mmWave MIMO systems is affected by the dependence on precise CSI.

Zhan and Dong [24] analysed the downlink multi-user massive MIMO system operating at mmWave and provided an interference cancellation (IC) framework for hybrid beamforming design. Three successive interference cancellation (SIC) assisted hybrid beamforming techniques were offered based on the proposed structure to handle intra- and inter-user interference. In particular, the first suggested technique employs SIC to cancel intra-user interference and zero-forcing (ZF) to cancel inter-user interference. In the second, intra-user interference was cancelled using ZF, and inter-user interference was cancelled using SIC. The third technique used SIC to decrease intra-user interference as well as inter-user interference. Moreover, the post-detection SINR determined the ideal detection sequence for data streams. However, the proposed algorithms are designed for flat fading mmWave channels and fully connected structures, which limits their applicability in wideband mmWave channels.

Muthukumaran [25] provided innovative techniques for efficient hybrid precoding and channel estimation in mmWave communication systems. Convolutional neural networks (CNNs) were used to solve the problems associated with channel estimation, and the Enhanced Whale Optimization Algorithm (EWOA) was used to optimize the network parameters. The suggested CNN-based channel estimating technique helped more effectively and simply estimate the channel in mmWave systems. Through the use of the EWOA optimization method during CNN training, the network parameters were adjusted to enhance the channel estimation process's precision and capacity for generalization. Moreover, adaptive RBFNN was used to produce hybrid precoding, which allowed for effective precoding while reducing complexity. However, this limits their applicability in wideband mmWave channels.

Previous studies have highlighted several limitations. First, the hardware design and computational complexity for this structure are prohibitively expensive [16]. Second, increasing the number of data streams per user raises interference levels and may cause crosstalk between users [17]. Third, the

proposed approaches are sensitive to channel condition variations [18]. Fourth, the scalability of the framework must be assessed for larger and more sophisticated communication systems [19]. Fifth, although massive MIMO systems are designed to support a large number of antennas, the scalability of the PSIA technique remains a concern [20]. Sixth, the sequential approximation approach requires iterative optimization at each level, and convergence is often difficult to achieve [21]. Additionally, scalability to more complex networks must be evaluated [22]. Moreover, reliance on accurate CSI limits beamforming performance in dynamic scenarios [23] and restricts applicability in wideband mmWave channels [24, 25]. Therefore, an innovative method is needed to address these issues and to systematically evaluate the performance of the proposed beamforming technique.

## 3. RECURRENT FORCING FOURIER PHASE DISTORTIONLESS RESPONSE NETWORK FOR MODERN MOBILE NETWORKS

mmWave communication systems, which operate at frequencies ranging from 30 to 300 GHz, have higher data speed and greater bandwidth, making them innovators for fifth-generation (5G) wireless networks. However, problems develop in situations with dense scatters, where multi-path fading causes destructive interference. To overcome these issues in multi-user mmWave massive MIMO Systems, a unique solution named Recurrent Butler Forcing Attenuators Fourier phase Distortionless Response Network is proposed. In advanced beamforming techniques, overcoming the impact of out-of-phase dispersed signals remains difficult. Multi-path fading generates delayed signal versions, resulting in ISI. Varying signal arrival delays worsen interference between signals, resulting in overlapping symbols at the receiver. These distortions impede proper demodulation, resulting in decoding errors and a considerable performance impact. The Amalgam Butler Zero Forcing Matrix is intended to address the issues caused by multi-path fading and destructive interference in extensively distributed situations. In this, the Butler matrix improves beamforming by integrating signals from several antennas, and the zero-forcing method decreases ISI by removing delayed versions of transmitted signals, which improves the changes in signal arrival timings induced by multi-path fading. Incorporating this matrix into the RNN's first layer enables the network to adapt to dynamic interference patterns, enhancing accurate demodulation and reducing decoding errors.

Also, effective angular resolution is necessary for reducing interference by steering beams away from undesirable directions. However, varying angular resolution with signal frequency complicates maintaining consistent performance across a wide band. This fluctuation results in inconsistent performance across different frequency components, affecting overall system reliability. Thus, DAFT is introduced to address varying angular resolution. It uses attenuators to adjust signal amplitudes, mitigating multi-path fading and interference. FFT is then used to analyse the signals for frequency-domain analysis. The DAFT technique is integrated into the RNN's second layer. It allows the network to learn spatial-temporal features and adapt to interference patterns. This ensures consistent performance across the full bandwidth

Moreover, beamforming algorithms are interfered with and noise is added by CTI, which is caused by the coexistence of numerous wireless technologies in one area. This interference results in beamforming systems generating inaccurate patterns. To tackle CTI in environments with multiple wireless technologies, the PTVSR is introduced. This method uses RNN's temporal dependencies to dynamically adapt to the changing wireless landscape. The phase shifter is introduced to adjust incoming signal phases and the MVDR algorithm optimally combines these adjusted signals, the system suppresses noise and enhances beamforming accuracy. Embedding this solution into the third RNN layer allows the system to effectively learn and adapt to complex signal interactions, mitigating CTI-induced inaccuracies and producing precise beam patterns in multi-technology environments.

Figure 1 illustrates the overall architecture of the proposed model. Three essential elements are included across the architecture's levels to improve system performance overall. First, the Amalgam Butler Zero Forcing Matrix addresses multi-path fading and destructive interference by maximizing beamforming and reducing ISI. It is included in the RNN's first layer and allows for dynamic response to interference patterns. Second, the second RNN layer incorporates the DAFT approach, which dynamically modifies signal amplitudes to reduce angular resolution fluctuations between frequencies. This makes it easier to learn spatial-temporal features, which is essential for reliable performance over the bandwidth. Lastly, the PTVSR in the third RNN layer uses the MVDR algorithm to combine signals optimally and modify the phases of the signals to solve CTI.

### 3.1 Amalgam Butler Zero Forcing Matrix

A unique technique called the Amalgam Butler Zero Forcing Matrix is intended to tackle the problems that arise in mmWave communication systems, especially in high-scatterer situations where destructive interference and multi-path fading are prevalent. The Butler matrix and the zero-forcing method are the two essential elements combined in the Amalgam Butler Zero-forcing matrix.

#### 3.1.1 Butler matrix

To provide an optimized beamforming Butler matrix is used, which produces constructive interference at the intended receiver position by adjusting the phase and amplitude of signals from each antenna element. It is well-suited for this research because of its effective nature for integrating signals from various antennas while providing spatial beamforming, which is essential for increasing signal quality and minimizing interference. Figure 2 shows the architecture of the butler matrix. A uniform rectangular array is used here. The Butler matrix is a beamforming network that consists of crossover, phase shifters, and hybrid couplers. The Butler matrix contains input ports and output ports. The system receives signals from multiple antennas. The input signals are fed into hybrid couplers, passive devices that split the incoming signals into two equal parts. Each path corresponds to a specific beam direction. Each of the split signals goes through phase shifters. The signals originating from various antennas are subjected to controlled phase shifts due to these phase shifters. In the desired direction, signals from various antennas are constructively (in-phase) aligned to reinforce each other by controlling these phase shifts suitably, while signals from other directions diminish because of destructive interference (out-of-phase).

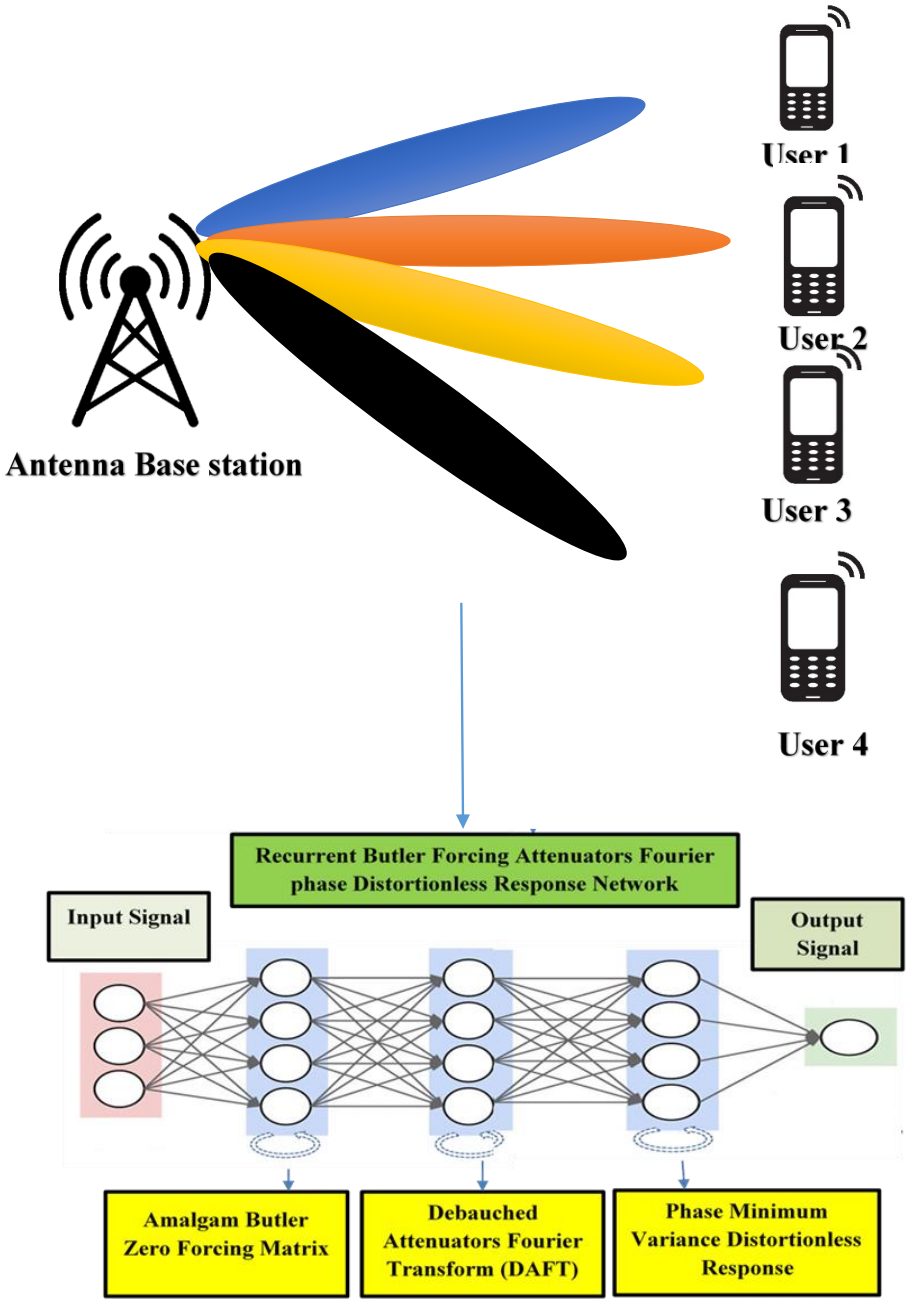


**Figure 1.** Overall architecture diagram of the proposed model

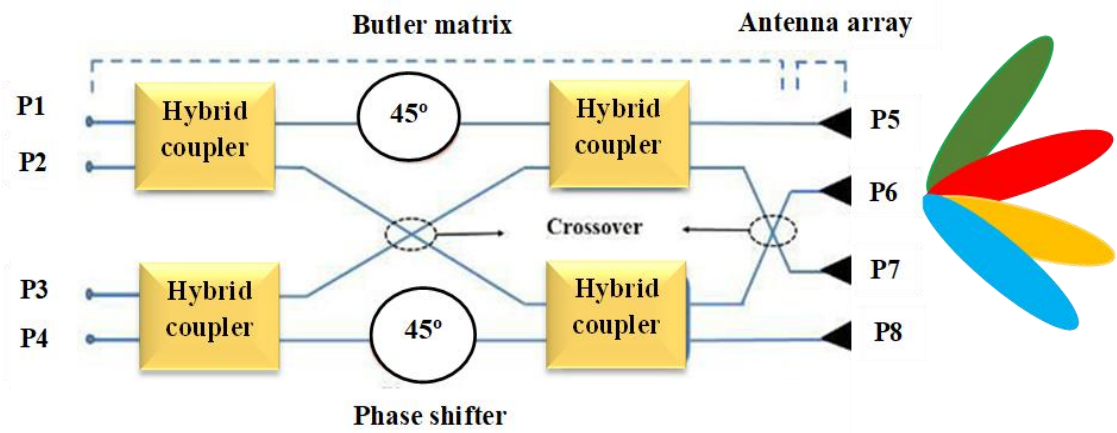


**Figure 2.** Architecture of Butler matrix

After passing through the phase shifters, the signals are combined using a crossover network. The signals are combined in such a way that they reinforce each other in the desired direction and cancel out in other directions, thereby forming a directive radiation pattern. The Butler Matrix efficiently combines signals from multiple beams, allowing simultaneous transmission to multiple users. By controlling the phase and amplitude of the signals from each antenna element, the Butler matrix optimizes beamforming to mitigate the impact of out-of-phase scattered signals. This helps in focusing the transmitted energy towards the desired receiver and reducing interference from other directions.

3.1.2. Zero-forcing algorithm

To further enhance performance, the Butler matrix output is further processed using a zero-forcing algorithm. The zero-forcing technique is used to reduce ISI by cancelling out the interference created by delayed replays of the transmitted signal. The zero-forcing algorithm, due to its simplicity and effectiveness in nullifying interference in environments with heavy scatters, is most suitable for this research. It works by creating an inverse filter that causes the received signal to match the transmitted signal at precise times, thereby wiping out interference from previous signals. Let denote the received signal $(y)$ be represented as in Eq. (1), which is the convolution of the transmitted signal $(x)$ and the channel impulse response $(h)$, corrupted by additive noise $n$. The zero-forcing beamforming matrix is derived by inverting the channel matrix to eliminate inter-user interference. The received signal is,

$$y = h * x + n \tag{1}$$

Then zero-forcing equalizer estimates the transmitted signal $x$ from the received signal $y$. This channel response includes the effects of multi-path fading and delays.

$$\hat{x} = Wy \tag{2}$$

where, $\hat{x}$ $i$s the estimated transmitted symbol vector. Using the estimated interference, the Zero Forcing algorithm designs a filter that nullifies the interference while preserving the desired signal. It does this by applying a filter matrix (Zero Forcing matrix) $W_{ZF}$ to the received signal, which is expressed in the following Eq. (3). To null interference, $ZF$ finds a weight matrix W such that $HW = I$ Using the Moore-Penrose pseudo-inverse:

$$W_{ZF} = (H^*H)^{-1}H^* \tag{3}$$

where, $H$ is the channel matrix. By applying the zero-forcing matrix $W_{ZF}$ to the received signal vector $y$. This ensures $HW_{ZF} = I$, perfectly decoupling user streams under ideal conditions. The filter is made to reverse the channel matrix's effects on the received signal, effectively cancelling out interference from delayed transmissions. By doing so, interference from previous signals is also effectively eliminated, lowering ISI and increasing the receiver's ability to detect signals accurately.

To enhance the system's adaptability to dynamic interference patterns, the Amalgam Butler Zero-Forcing Matrix is incorporated into the first layer of an RNN. Each neuron in the first layer of the RNN corresponds to an element in the Butler Zero Forcing Matrix. The hidden state of this first layer is expressed in the following Eq. (4)

$$K_t{}^1 = \sigma(W_{KK}{}^1 K_{t-1}{}^1 + W_{xK}{}^1 W_{ZF} + B_K{}^1) \tag{4}$$

The RNN's capacity to keep a memory of previous inputs allows it to lessen the effects of ISI by learning to recognize and correct delayed transmissions. By processing sequential data representing received signals over time, the RNN effectively captures the temporal variations caused by multi-path fading and interference. This is essential for correctly demodulating and retrieving original signals from distorted waveforms under challenging propagation conditions.

### 3.2 Debauched Attenuators Fourier Transform (DAFT) for consistent angular resolution

In mmWave communication systems, the problems caused by differing angular resolution across a wide frequency range are tackled using the DAFT, which is incorporated in the RNN's second layer. The RNN first layer output is given to the DAFT.

In DAFT initially, attenuators are used, which dynamically adjust the amplitudes of incoming signals. The attenuators continuously monitor the incoming signals to identify their characteristics, such as signal intensity and interference. Based on the detected signal characteristics, the attenuators are dynamically adjusted to modify the amplitudes of the signals. The attenuator reduces the amplitude of a signal that is too strong, while allowing more of the signal to pass through without attenuation.

As the signals travel through attenuators, their amplitudes are changed in real-time. This dynamic attenuation reduces the impacts of multi-path fading by adjusting for signal variations generated by reflections and diffraction. Attenuators also assist in mitigating the effects of destructive interference by altering signal intensities. This adjustment reduces interference produced by signals from unexpected directions or other sources operating in the same frequency range. Attenuators improve the overall quality of signals received by dynamically changing their amplitudes. By dynamically adjusting signal amplitudes, DAFT helps in maintaining more consistent angular resolutions across different frequency components.

After signal amplitude adjustment by attenuators, the signals are processed using the Fast Fourier Transform (FFT). FFT converts the time-domain signals into the frequency domain, allowing for frequency-domain analysis. The ability of FFT to efficiently compute the DFT of a sequence makes it suited for this research, especially in scenarios where a high number of frequency components need to be analysed at the same time.

The input to the FFT is a sequence of $N$ complex numbers $x[n]$, where $n = 0,1,\ldots,N-1$. This sequence represents sampled signal values in the time domain. FFT employs a divide-and-conquer strategy to efficiently compute the frequency components of the input signal. Divide the sequence $x(n)$ into two smaller sequences, one for the even-indexed items $x_e[m] = x[2m]$ and the other for the odd-indexed elements $x_o[m] = x[2m+1]$. Recursively apply the FFT to the even-indexed and odd-indexed sequences, which are expressed in the following Eqs. (5) and (6)

$$X_e[k] = \sum_{m=0}^{\frac{N}{2}-1} x_e(m) e^{-j\frac{2\pi}{N/2}km} \tag{5}$$

$$X_o[k] = \sum_{m=0}^{\frac{N}{2}-1} x_o(m) e^{-j\frac{2\pi}{N/2}km} \quad (6)$$

After recursively computing the FFTs of the smaller sequences (denote the results as $(X_o[k], X_e[k])$, combine them to get the FFT of the original sequence. Combine the results of the smaller FFTs to form the FFT of the original sequence, using the following Eqs. (7) and (8).

$$X(k) = X_e[k] + W_N^k \cdot X_o[k] \quad (7)$$

$$(k + N/2) = X_e[k] - W_N^k \cdot X_o[k] \quad (8)$$

The FFT algorithm calculates the frequency-domain representation of the signal. The formula for the FFT is given by the following Eq. (9)

$$X(k) = \sum_{n=0}^{N-1} x(n) e^{-j\frac{2\pi}{n}kn} \quad (9)$$

where, $x(n)$ is the time-domain signal, $X(k)$ is the frequency-domain representation, $N$ is the number of points in FFT, and $j$ is the imaginary unit. Then the results to obtain the overall frequency spectrum. The resulting sequence $X[k]$ represents the frequency-domain transformation of the original sequence $x[n]$. It reveals how different frequency components are distributed in the signal. FFT provides a frequency-domain representation that allows for the analysis of different frequency components. Using FFT to analyse the data in the frequency domain allows for the capture of the various angular resolutions since different angular resolutions correlate to distinct frequency components in the received signal. The algorithm for FFT is given below in Algorithm 1.

**Algorithm 1: FFT**

**Input:** A sequence $x[n]$ of length N

**1.** Initialization: Start with a sequence $x[n]$ of length N.

**2.** Divide the Sequence

Separate the sequence x into two sub-sequences $x_e[m]$ containing the elements at even indices.

$x_o[m]$ containing the elements at odd indices

**3.** Recursive FFT**:**

Recursively compute the FFT of the even-indexed elements $(X_e[k])$

Recursively compute the FFT of the odd-indexed elements $(X_o[k])$

**4.** Combine the Results**:**

Initialize an empty array $X[k]$ of length N to store the final FFT results.

Combine the results

**5.** Return the Result**:**

Return the array $X[k]$ containing the frequency-domain representation of the input sequence $x[n]$.

**Output:** The frequency-domain representation $X[k]$ of the input sequence $x[n]$.

Figure 3 presents the flow diagram of DAFT. The process starts with acquiring the raw input signal, which is fed into the first layer of a Recurrent Neural Network (RNN) to capture temporal dependencies. This initial processing prepares the data for refinement. Next, the signal undergoes dynamic amplitude adjustments to enhance relevant features and suppress noise. The conditioned signal is then passed to the FFT module. The FFT operates using a divide-and-conquer strategy, recursively breaking the signal into smaller parts. Each segment is transformed individually, and the results are efficiently combined. This yields a complete frequency domain representation. The output reveals essential frequency components for further analysis. The process integrates RNN-based temporal modelling with FFT-based spectral analysis.

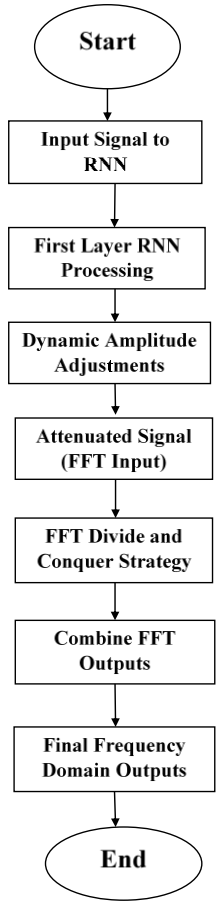


**Figure 3.** Flow diagram of DAFT

This DAFT is integrated into the second layer of the RNN, this layer captures spatial-temporal features and mitigates interference patterns due to varying angular resolutions. RNNs learn to recognize and adapt to spatial and temporal patterns in signal data. Spatial patterns include the direction of signal arrival, whereas temporal patterns comprise variations in signal amplitude or interference over time. The RNN's hidden states encode these patterns, allowing the network to discriminate between various signal sources and reduce interference. The RNN hidden state can be expressed as in Eq. (10):

$$K_t^2 = \sigma({W_{KK}}^2 {K_t}^1 + {W_{xK}}^2 X(k) + {B_K}^2) \quad (10)$$

The RNN adjusts its hidden state depending on the input signal at each time step, taking into account the previous hidden state as well as details about the received signals, such as their frequencies and angular resolutions. The adaptive nature of the RNN ensures consistent performance across the entire bandwidth. It continuously learns and adapts to changing conditions, maintaining optimal signal quality.

With the use of dynamic attenuators and FFT, along with an RNN for beamforming, the DAFT approach efficiently manages wide frequency spectrums and different angular resolutions. This hybrid approach improves the system's

capacity to adjust to intricate interference patterns while simultaneously reducing destructive interference and multi-path fading, guaranteeing reliable and steady operation.

### 3.3 PTVSR for CTI

The PTVSR is an innovative method for addressing in environments where various wireless technologies coexist, such as Wi-Fi and Bluetooth. This method uses an advanced phase shifter and MVDR beamforming inside an RNN's third layer

In PTVSR, initially phase shifter is introduced to adjust the phase of incoming signals. The system first examines the presence of interference in the received signals. When signals from various wireless technologies operate in the same environment, they can interfere with one another due to mismatches in their frequencies, amplitudes, and phases. Interfering signals vary in strength and amplitude compared to the desired signals. By measuring the strength of received signals across different frequency bands, the system identifies the presence of interference. When interference is identified, the phase shifter dynamically modifies the incoming signal's phase. The purpose of this adjustment is to minimize the effect of conflicting signals while optimizing the signal's alignment with the intended beamforming direction. This phase adjustment process is mathematically represented in Eq. (11).

$$x'(t) = x(t) \times e^{j\phi} \tag{11}$$

where, $x'(t)$ represents the phase-shifted signal, $x(t)$ is the incoming signal, and $\phi$ denotes the phase shift angle. The phase shifter applies a controlled delay to the incoming signal to ensure proper operation. This delay changes the phase of the signal waveform and alters the phase of the signals. Further, the phase shifter helps to spatially separate the desired signal from interfering signals, thereby enhancing the signal-to-interference ratio.

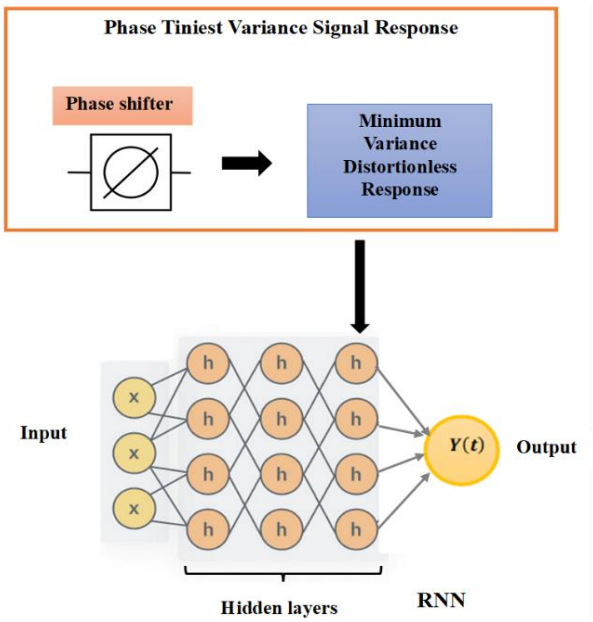


**Figure 4.** Block diagram of PTVSR

Figure 4 illustrates the block diagram of PVSR. After phase adjustment, the signals are fed into the MVDR beamformer. The adaptability and noise suppression properties of WVDR are discussed in this section. The MVDR algorithm optimally combines the phase-adjusted signals to form a beam that minimizes interference and noise while maintaining the integrity of the desired signal. Let $y(t)$ denote the received signal vector at the time $t$. The first step in the MVDR algorithm is to compute the covariance matrix $C$ from the received signals. The statistical correlations between the received signals at various sensor components are represented mathematically by the covariance matrix. The covariance matrix $C$ is calculated as follows in Eq. (12):

$$C = \frac{1}{N}\sum_{n=1}^{N} x'(t)x'^{H}(t) \tag{12}$$

where, $N$ is the number of signals, $x'^{(t)}$ is the vector of received signals at a time $t$, and $H$ is the hermitian transpose. Following that, the optimal beamforming weights $w_M$, are calculated using the MVDR algorithm.

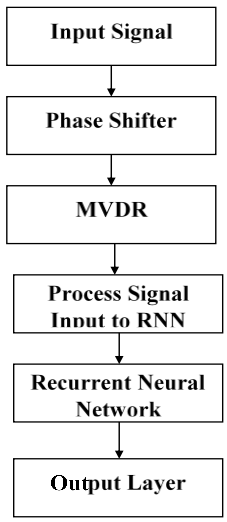


**Figure 5.** Flowchart of PTVSR

The flowchart of PTVSR is depicted in Figure 5. The process begins by adjusting the input signal's phase using a phase shifter. It then passes through the MVDR filter, which minimizes noise while preserving essential features. The refined signal is formatted and delivered to a RNN. The RNN's hidden layers learn and analyse the signal's temporal patterns. Ultimately, the output layer generates the final prediction or response, represented as Y(t).

To minimize the array output power $P_w$ while ensuring unity gain in the direction of the desired signal, the corresponding steering vector is used, and the optimal weight vector is selected accordingly. The MVDR problem minimizes output power while preserving gain in the desired direction. The following is a possible syntax for the MVDR adaptive algorithm:

$$min_w\{w^H C w\} \quad subject\ to\ w^H a(\theta) = 1 \tag{13}$$

where, $a(\theta)$ is the steering vector. The next step involves calculating the spatial filter weights that optimize the beamforming performance. Mathematically, the MVDR weights vector $w_M$ is given by the following Eq. (14):

$$w_M = \frac{C^{-1}a(\theta)}{a^H(\theta)C^{-1}a(\theta)} \tag{14}$$

Finally, Multiplying the spatial filter vector $w_M$ by the received signal vector yields the MVDR beamformer's output, represented as $Y$, which is shown in Eq. (15)

$$Y = w^H x'(t) \tag{15}$$

MVDR dynamically adjusts to environmental changes by updating the beamformer weights using the spatial covariance matrix. By applying Lagrange multipliers, the solution is derived as follows:

$$w_{MVDR} = \frac{C^{-1}a(\theta)}{a^H(\theta)C^{-1}a(\theta)} \tag{16}$$

This allows it to mitigate interference from coexisting wireless technologies and produce more accurate beam patterns. In the PTVSR module, the phase shift angle $\phi$ is varied in the range $[-\pi, \pi]$, with a resolution of $0.1\pi$ radians. This dynamic range allows precise phase steering to mitigate CTI. In the DAFT module, the attenuators dynamically adapt within a 0-30 dB range. If the SNR falls below 20 dB, the attenuation is proportionally decreased based on the SNR level. The adjustment is governed by:

$$A(t) = A(t-1) + \alpha(S_{ref} - S_{measured}), \text{ with } \alpha = 0.05 \tag{17}$$

where, $S_{ref}$ is the reference signal strength. The algorithm for PTVSR is given in algorithm 2.

**Algorithm 2:** PTVSR

**Input:** Received signal vector $x(t)$ at time $t$, number of signals N, steering vector $a(\theta)$,

1. Initialization: Set phase shift angle $\phi = 0$.
2. Phase adjustment:
   For each incoming signal $x(t)$ do
   Calculate interference presence by measuring signal strength across frequency bands.
   **Adjust the phase of incoming signals using** $x'(t) = x(t) \times e^{j\phi}$
   End for
3. Compute Covariance Matrix:
   Calculate the covariance matrix $(C)$ of the phase-shifted signals using Eq. (12)
4. Calculate Optimal Beamforming Weights:
   Using Eq. (14)
5. **Apply Beamforming Weights:**
   Multiply the optimal weights by the received signal vector to form the beamformed output using Eq. (15)

**Output:** Produce the final beamformed signal $(Y)$ with minimized interference and noise.

The combined solution, comprising the phase shifter adjustment and MVDR-based beamforming, is embedded into the third layer of the RNN. This integration allows the system to learn and adapt to the complex interplay of signals over time. The third layer of the RNN will receive this combined solution if the hidden state update equation is modified as follows in Eq. (18):

$$K_t^3 = \sigma({W_{KK}}^3 {K_t}^2 + {W_{xK}}^3 Y + {B_K}^3) \tag{18}$$

The system makes use of the RNN's capacity to record temporal dependencies, allowing it to dynamically adapt to changing wireless sceneries. Finally, the RNN's output is generated based on the hidden state of the third layer, which is expressed in the following Eq. (19):

$$Y(t) = \sigma(W_Y K_t^3 + B_Y) \tag{19}$$

The output layer of the RNN generates demodulated symbols based on the learned representations from the hidden layers. These symbols represent the recovered information transmitted by different users, with reduced distortion and interference effects. Through the use of the RNN's capacity to acquire consecutive patterns, the network efficiently reduces errors caused by CTI and generates more accurate beam patterns. The RNN architecture's incorporation of the phase adjustment procedure and the MVDR algorithm improves the network's capacity to reduce interference and boost beamforming accuracy in situations with a variety of wireless technologies, such as Wi-Fi and Bluetooth, which improves performance in contexts with a variety of wireless technologies.

Overall, the proposed hybrid beamforming approach increased signal quality by lowering ISI effects, assuring constant performance over the whole spectrum, and mitigating interference from other wireless technologies.

## 4. RESULT AND DISCUSSION

This section contains a full description of the implementation findings and the proposed system's performance, as well as a comparison section to ensure that the proposed approach is appropriate for multi-user mmWave massive MIMO systems.

### 4.1 Experimental setup

The "Recurrent Butler Forcing Attenuators Fourier phase Distortionless Response Network" experimental setup for multi-user mmWave massive MIMO systems involves utilizing a uniform rectangular array configuration with 108 transmitting antennas and Number of RF chains is 54. In the hybrid beamforming setup, the number of RF chains is less than the number of transmitting antennas. The CSI is considered imperfect, reflecting real-world conditions. Speech signal samples, generated using a standard generator, are employed for training the neural network model. The dataset comprises 1000 different speech samples, which are split into a 9:1 ratio for training and testing, respectively. The proposed system is simulated in MATLAB, and this section includes an extensive discussion of the implementation results and performance, as well as a comparison section to confirm that the proposed setup functions properly. Table 1 represents the system configurations which are used to design the proposed model.

### 4.2 Simulated output of the proposed model

In this section, examine the analysis of simulation output from the proposed Recurrent Butler Forcing Attenuators Fourier phase Distortionless Response Network. This aims to provide constructive insights and interpretation of the simulation output.

DAFT results of magnitude and phase of the proposed model is shown in Figure 6. The magnitude of the signals varies significantly across the frequency index for each user.

The variations in amplitude indicate that the system dynamically adjusts the signal amplitudes to manage interference and optimize beamforming. The diverse amplitude responses suggest that DAFT effectively mitigates multi-path fading and destructive interference, enhancing spectral efficiency. The phase responses for each user vary widely across the frequency index. This indicates that the system is adjusting the phase of incoming signals dynamically to mitigate the impact of interference. The phase adjustments show the system's ability to handle varying angular resolutions across the frequency spectrum, crucial for maintaining high spectral efficiency.

**Table 1.** System configurations

| Components | Specifications |
|---|---|
| Software | MATLAB |
| OS | Windows 10 (64-bit) |
| Processor | Intel i5 |
| RAM | 8GB RAM |

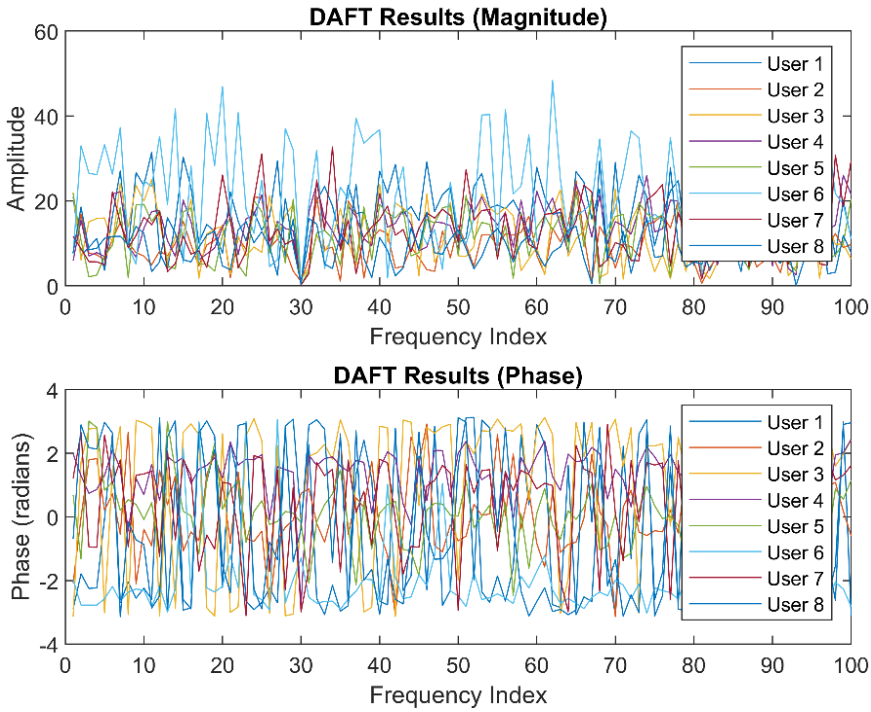


**Figure 6.** DAFT results of magnitude and phase

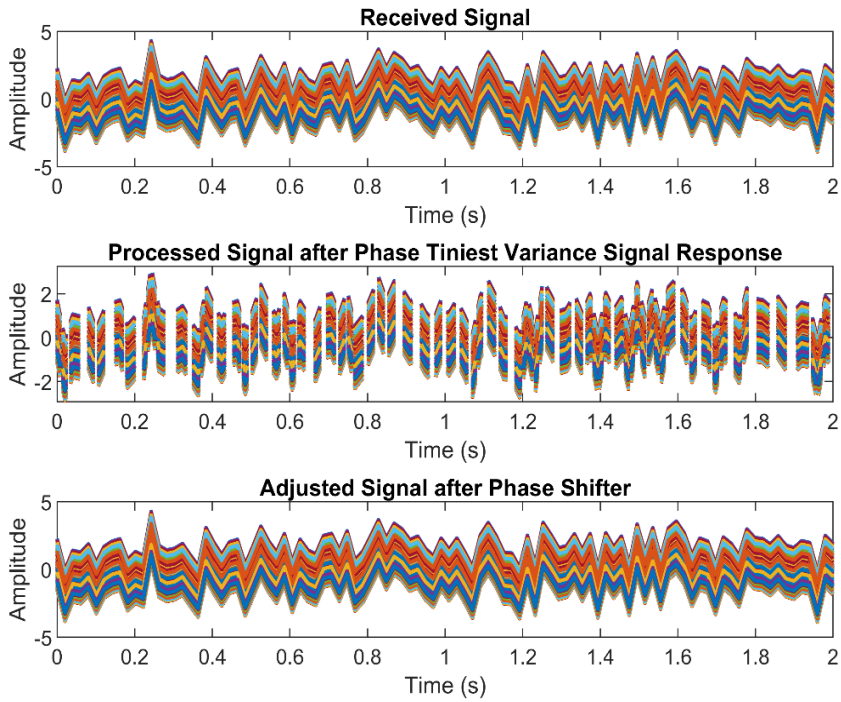


**Figure 7.** Adjusted and received signals

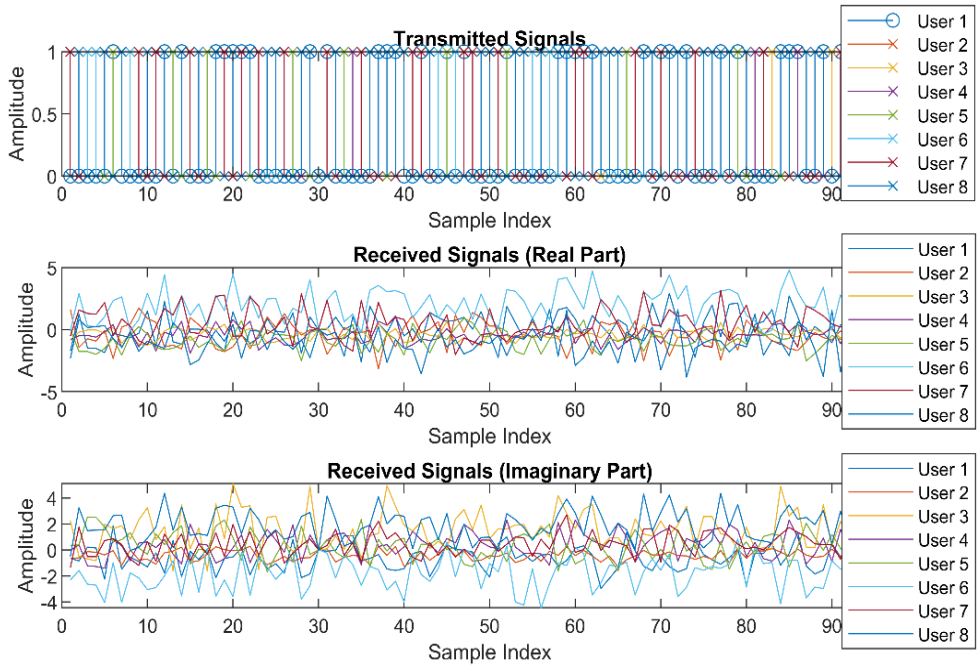


**Figure 8.** Transmitted and received signals

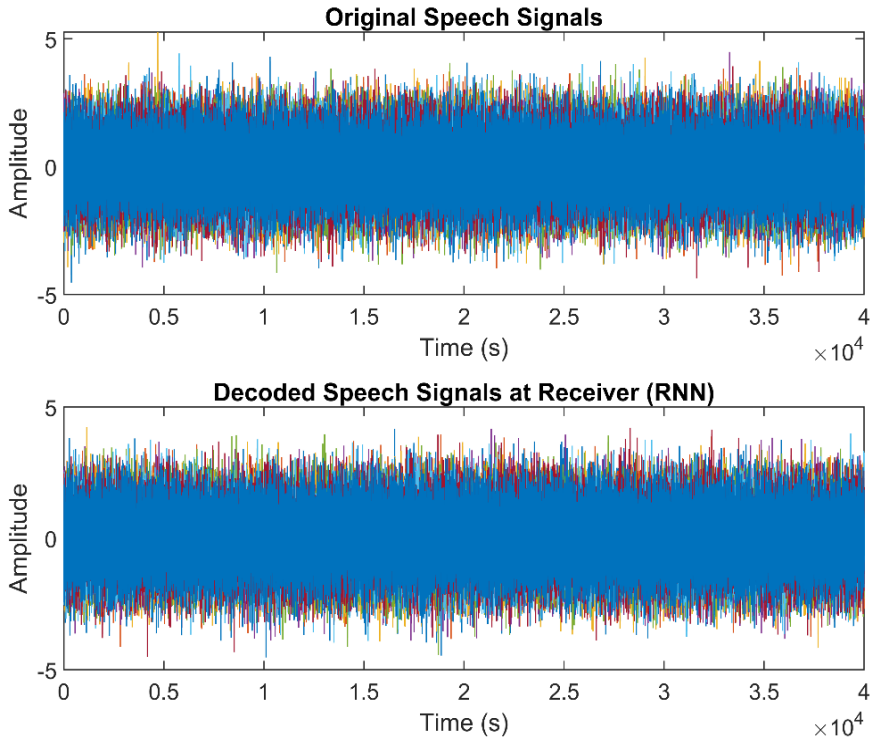


**Figure 9.** Original and decoded speech signal

Adjusted and received signals of the proposed model are expressed in Figure 7. The top plot shows the received signal. The signal amplitude fluctuates widely, indicating the presence of various out-of-phase components and interference. The next plot depicts the signal after applying the PTVSR technique. This method adjusts the signal phases to reduce interference effects. As a result, the amplitude variations are more confined, and the signal appears to be less distorted, demonstrating a reduction in CTI and noise. The last plot shows the signal after additional phase shifting. This phase adjustment aligns the signal components to further mitigate the effects of multi-path fading. The amplitude variations are smoother and more uniform, indicating improved signal coherence and reduced destructive interference.

Figure 8 illustrates the transmission and reception of signals for eight users in a multi-user mmWave massive MIMO system, depicting the effects of multi-path fading and interference. The transmitted signals for all users are uniform and consistent, showing that the system can handle multiple users transmitting simultaneously without initial interference. The real part of the received signals for each user is shown, demonstrating substantial amplitude variations and noise. The imaginary part of the received signals is also significantly distorted and noisy. The variations indicate the complex nature

of the received signals due to channel effects.

The above Figure 9 shows the original and decoded speech signal of the proposed model. The top plot illustrates the original speech signals, which fluctuate within the amplitude range of approximately -5 to 5 over a time of $4\times10^4$. These signals contain various frequencies and amplitudes, representing the natural variability in speech. The bottom plot shows the decoded speech signals at the receiver, also fluctuating within the same amplitude range of about -5 to 5 over the same time. This indicates that the RNN has successfully demodulated and reconstructed the speech signals with high fidelity, preserving the integrity and quality of the original audio.

### 4.3 Performance analysis of the proposed model

This section provides an extensive investigation of the proposed multi-user mmWave massive MIMO systems, focusing on its robustness, accuracy, and efficiency. The performance of the approach is measured using a range of metrics and benchmarks, which allows for a comprehensive examination and confirmation of its efficacy in beamforming.

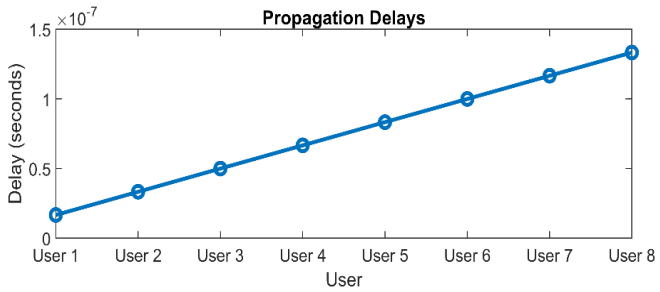


**Figure 10.** Propagation delays vs users

The Figure 10 illustrates the propagation delays experienced by different users in the system, as the number of users increases. For 1 user, the proposed approach has a delay of 0.2 seconds, and as the number of users increases to 8 the delay of the proposed system increases to 1.3 seconds. The PTVSR approach dynamically adjusts the phase of incoming signals to reduce interference and propagation delays.

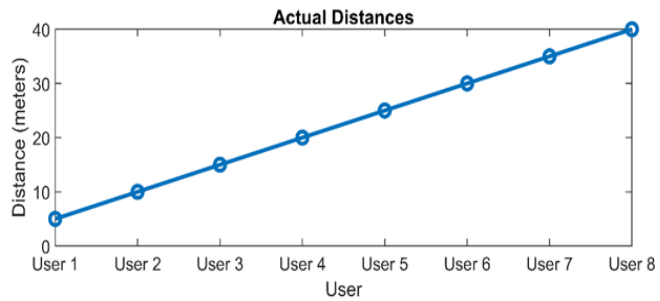


**Figure 11.** Actual distance vs users

The actual distances between the users are shown in Figure 11, which increases linearly as the number increases. For user 1, the proposed approach has an exact distance of 5 meters, and when the number of users increases to 8, the actual distance of the proposed system rises to 40 meters. As the number of user's changes or as users move, the PTVSR adaptively mitigates interference, leading to more precise beam patterns and improved performance across different distances.

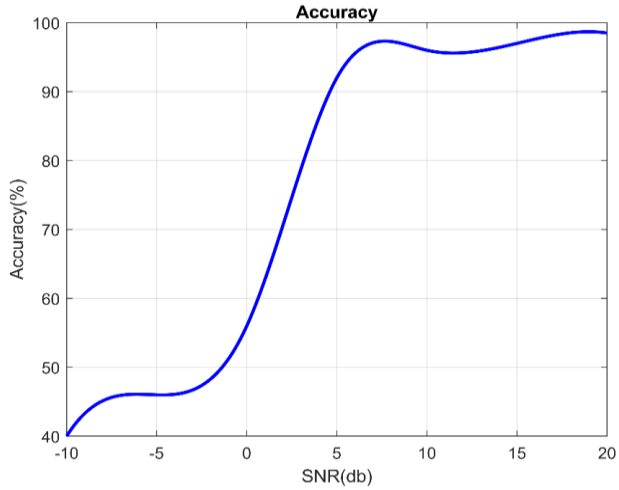


**Figure 12.** Accuracy of the proposed model

The above Figure 12 illustrates the accuracy of the proposed model. When the SNR value is -10db, the proposed approach achieves a minimum accuracy of 40%, whereas when the SNR value is 20db, it achieves a maximum accuracy of 99.2%. The phase shifter and MVDR algorithm improve accuracy by dynamically adapting to changing wireless landscapes and optimally combining adjusted signals to suppress noise, enhancing the accuracy of beamforming.

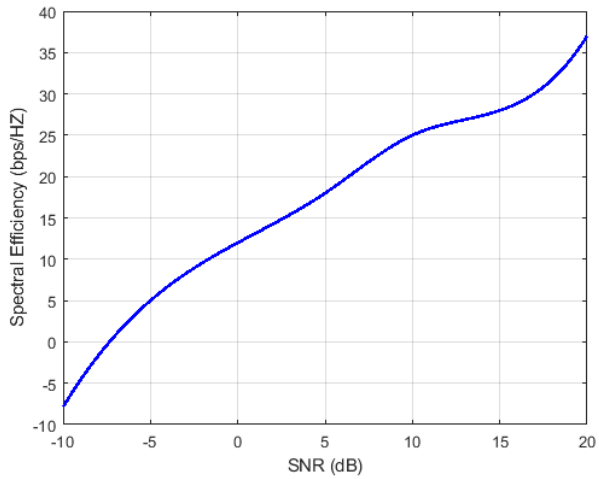


**Figure 13.** Spectral efficiency vs SNR

Figure 13 depicts the spectral efficiency of the proposed model vs SNR. The proposed approach has a low spectrum efficiency of -7.5 bps/Hz at -10db SNR, however, it achieves its best spectral efficiency value of 37 bps/Hz at 20db SNR. DAFT enhances spectral efficiency by dynamically adjusting signal amplitudes to mitigate the impact of multi-path fading and destructive interference.

Figure 14 shows the spectral efficiency (in bits/s/Hz) versus the number of users (ranging from 1 to 8) in the proposed system. The spectral efficiency remains constant at approximately 9.25 bits/s/Hz across all users from 1 to 8. The adaptive spatial-temporal features learned by the RNN further support consistent performance by capturing and mitigating interference patterns across different user scenarios.

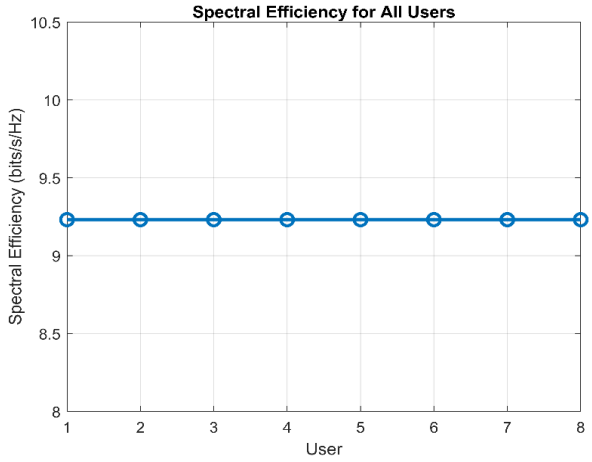


**Figure 14.** Spectral efficiency for all users

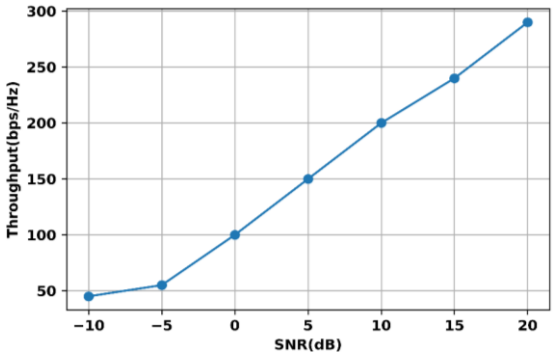


**Figure 15.** Throughput of the proposed model

The above Figure 15 illustrates the throughput of the proposed model. When the SNR value increases the throughput of the proposed model also, increases. When the SNR value is -10db the proposed model achieves a minimum throughput value of 50bps/Hz, whereas the proposed model achieves a maximum throughput value of 290bps/Hz when the SNR value is 20db. FFT allows for better frequency-domain analysis, leading to more efficient data processing and higher throughput

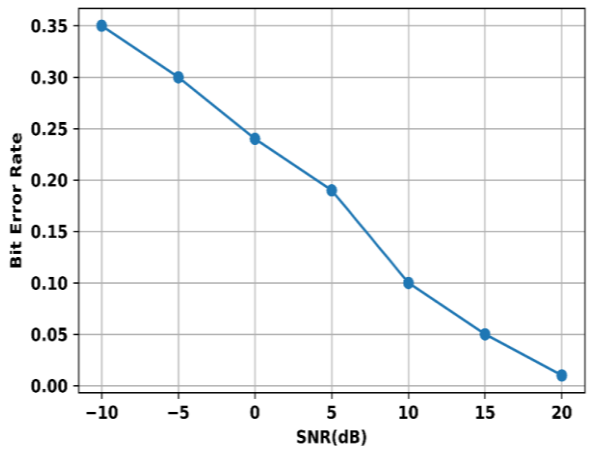


**Figure 16.** Bit error rate of the proposed model

Figure 16 illustrates the bit error rate of the proposed model. When the SNR value is -10db the proposed model achieves a maximum bit error rate value of 0.35, whereas the proposed model achieves a minimum bit error rate of 0.01, when the SNR value is 20db.The zero-forcing algorithm minimizes ISI, reducing BER by defeating delayed versions of the transmitted signal and improving variations in signal arrival times induced by multi-path fading.

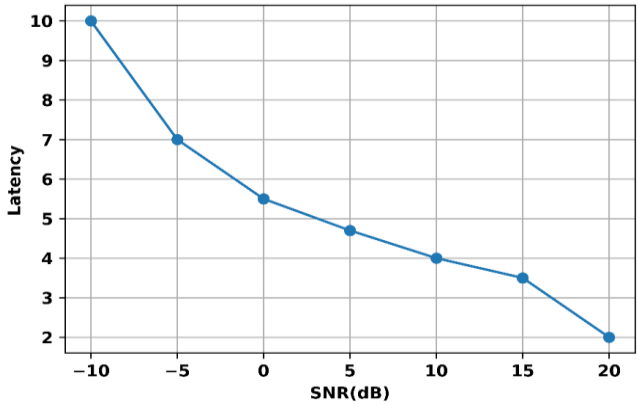


**Figure 17.** Latency of the proposed model

The latency performance of the proposed model is shown in Figure 17. The proposed approach achieves a minimum latency value of 2 when the SNR value is 20db, and a maximum latency value of 10 when the SNR value is -10db. The adaptive learning capabilities of the RNN in handling CTI reduce latency by ensuring quick adaptation to changing interference patterns.

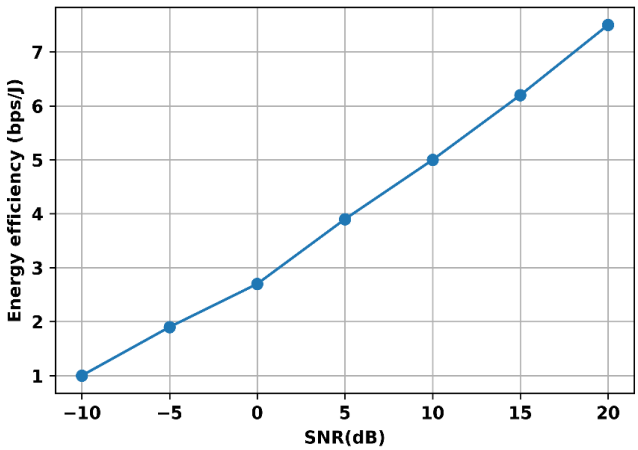


**Figure 18.** Energy efficiency of the proposed model

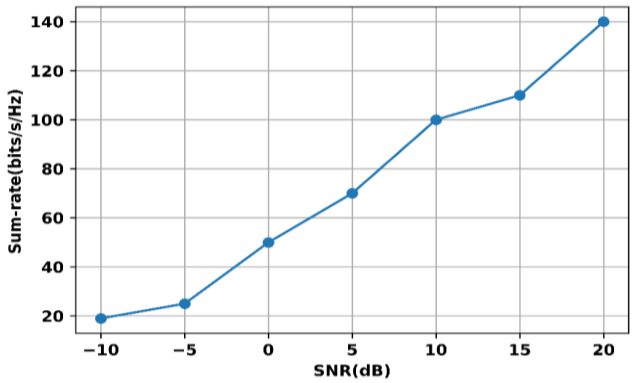


**Figure 19.** Sum rate of the proposed model

The above Figure 18 illustrates the energy efficiency of the proposed model. The proposed model achieves a minimum energy efficiency of 1 bps/J and a maximum energy efficiency

of 7.5 bps/J when the SNR value is -10 and 20 dB respectively. By mitigating interference and distortion more effectively, the DAFT system can transmit data more reliably using less energy, leading to improved energy efficiency.

The proposed model sum rate is expressed in the Figure 19. The proposed model attains a maximum sum rate of 140 bits/s/Hz when the SNR value is as high as 20 dB. Also, achieves a minimum sum rate of 20 bits/s/Hz, when the SNR value is as low as -10dB. By suppressing interference and noise, the PTVSR increases the effective capacity of the system and thus improves the sum rate.

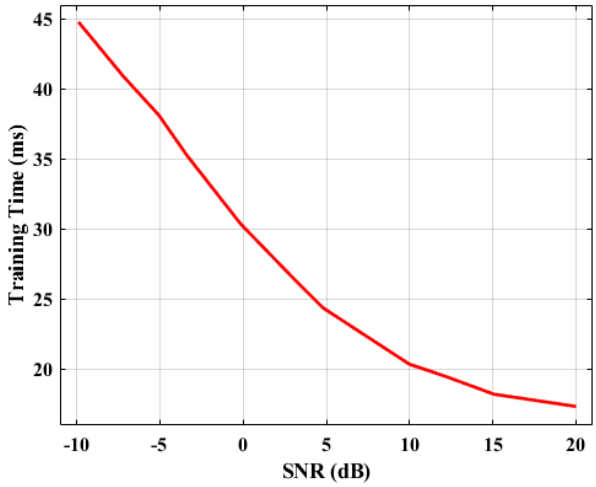


**Figure 20.** Training time of the proposed model

Figure 20 illustrates how Signal-to-Noise Ratio (SNR) affects model training time. When the SNR is low, such as -10 dB, the training time is highest, reaching around 45 milliseconds. As the SNR increases, the training time decreases steadily, indicating that the model trains more efficiently with cleaner signals. Around 10 dB, the training time falls below 20 milliseconds, and it continues to decrease slightly as SNR reaches 20 dB. This trend highlights the significant impact of signal quality on training performance, showing that higher SNRs lead to faster convergence and reduced computational effort.

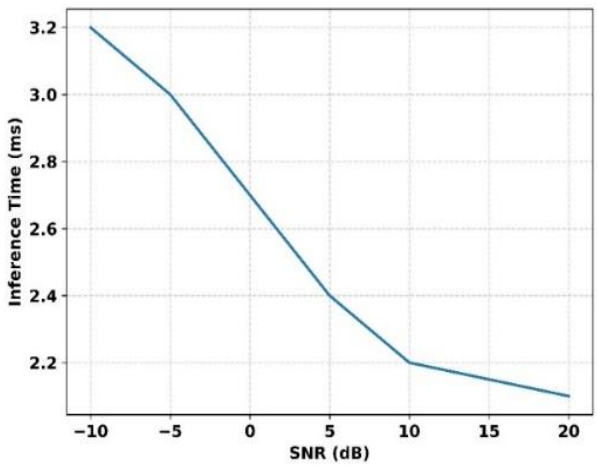


**Figure 21.** Inference time of the proposed model

Figure 21 demonstrates that inference time decreases as the SNR increases. At low SNR levels, such as -10 dB, the inference time is highest, around 3.2 milliseconds. As the signal becomes clearer with increasing SNR, the inference time steadily drops, reaching approximately 2.1 milliseconds at 20 dB. This trend indicates that higher signal quality reduces the computational burden during inference, allowing the model to process inputs more efficiently and quickly. The improvement is especially noticeable between -10 dB and 10 dB, where inference time drops sharply. This suggests that optimizing signal conditions can significantly enhance real-time model performance.

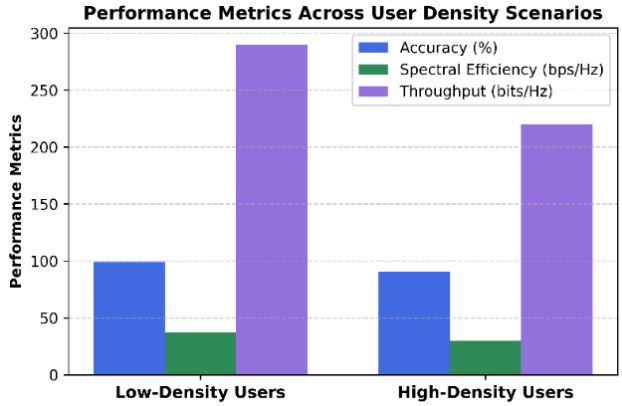


**Figure 22.** Performance metrices across high density users scenario

The performance metric under a high-density user scenario is represented in Figure 22. In contrast, low-density users achieve a higher throughput of approximately 290 bits/Hz and an accuracy close to 100%, compared to high-density users. Spectral efficiency shows a slight decline, decreasing from around 35 bps/Hz to 30 bps/Hz as user density increases. The performance drop in high-density environments is attributed to intensified inter-user interference. Despite this, the proposed method demonstrates resilience and maintains robust performance across varying user densities. This robustness highlights its adaptability for future high-capacity networks. Additionally, latency remains within acceptable limits, ensuring quality of service is preserved even under load.

### 4.4 Comparative analysis of the proposed model

This section highlights the proposed method's performance by comparing it to the outcomes of existing approaches showing their results based on various metrics such as accuracy, spectral efficiency, throughput, BER, sum rate, and energy consumption.

The proposed method's accuracy is contrasted with that of other approaches, as shown in Figure 23. The various methods such as OMP, LMS, and CNN achieve an accuracy value of 79%, 80%, and 98.7% respectively, when the SNR value is 20dB. The accuracy values of the RNN are 99.2%, respectively. This suggests that RNN outperforms CNN in terms of accuracy.

The spectral efficiency achieved by the proposed technique is compared with other approaches illustrated in Figure 24. The other approaches such as OMP, LMS, and CNN achieve a low spectral efficiency value of 30 bps/Hz, 34 bps/Hz, and 33.8 bps/Hz. Also, compared with existing models the proposed model RNN achieves the highest spectral efficiency value of 37 bps/Hz, when the SNR value is 20dB. This indicates that RNN has a significantly greater spectral efficiency than CNN.

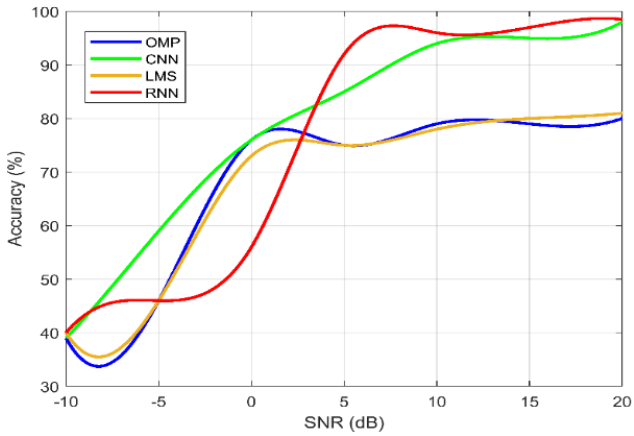


**Figure 23.** Comparison of accuracy

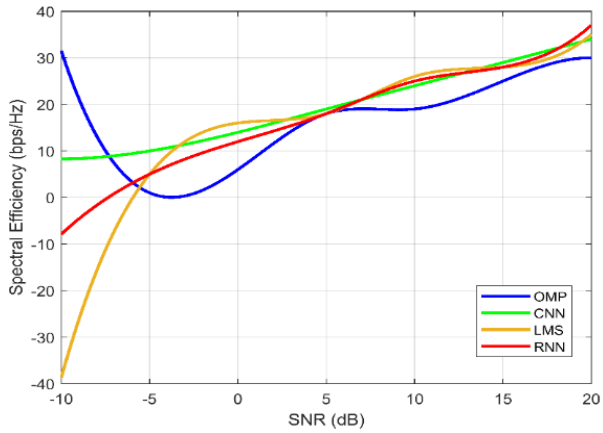


**Figure 24.** Comparison of spectral efficiency

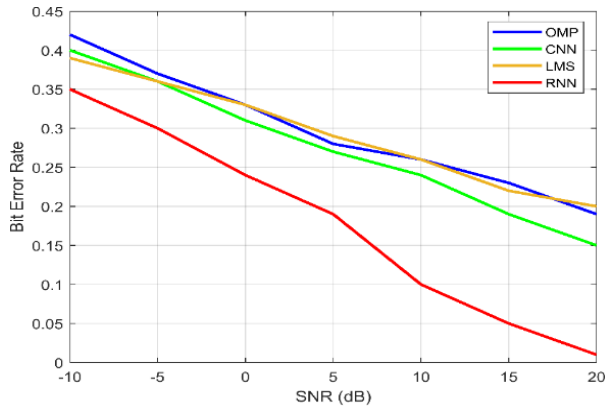


**Figure 25.** Comparison of Bit Error Rate (BER)

The BER achieved by the proposed technique is compared with other approaches illustrated in Figure 25. The other approaches such as OMP [28], LMS [29], and CNN achieve a low BER value of 0.19, 0.2, and 0.15, and RNN has a low BER value of 0.01 when the SNR is 20 dB Also, compared with existing models the proposed model RNN achieves the lowest BER value.

The energy efficiency comparison of the proposed model with existing models is shown in Figure 26. The existing models such as OMP, CNN, and LMS achieve energy efficiency of 1.6 bits/J, 6.3 bits/J, and 2 bits/J respectively, when the high SNR of 20dB. The proposed RNN model outperforms existing models, this achieves an energy efficiency value of 7.5 bits/J.

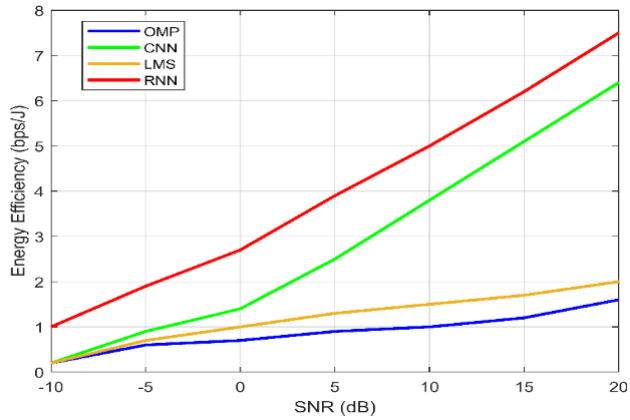


**Figure 26.** Energy efficiency comparison

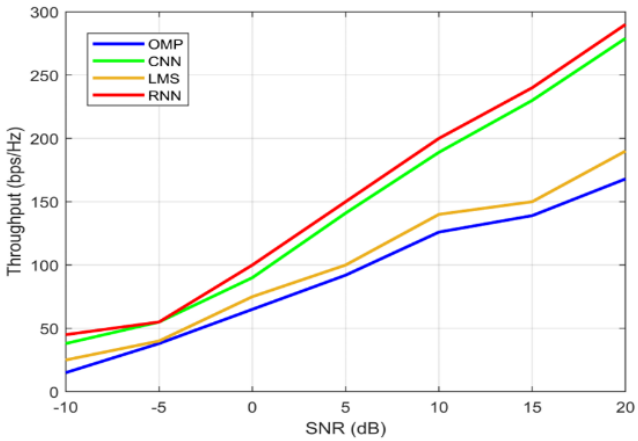


**Figure 27.** Comparison of throughput

The throughput comparison of the proposed model is illustrated in the Figure 27. The existing models OMP, CNN, and LMS attain a throughput value of 165 bits/Hz, 275 bits/Hz, and 185 bits/Hz, respectively. Compared with existing beamforming techniques the proposed RNN method achieves a high throughput value of 290 bits/Hz.

Table 2 provides a comparative analysis of the proposed RNN model against traditional methods such as OMP, LMS, and CNN across five performance metrics, namely accuracy, BER, spectral efficiency, throughput, and energy efficiency. The OMP method shows the lowest accuracy at 79% with high BER (0.19), while LMS marginally improves on both. CNN demonstrates significant improvements, achieving 98.7% accuracy and reduced BER (0.15). However, the proposed RNN surpasses all methods, achieving the highest accuracy of 99.2%, the lowest BER of 0.01, and superior spectral efficiency (37 bps/Hz) and throughput (290 bits/Hz). It also leads in energy efficiency at 7.5 bits/J, highlighting its robustness and practical efficiency in high-performance mmWave communication scenarios.

Overall, the proposed approach demonstrates that it is more effective and accurate when compared to previous. The proposed model attains a high accuracy of 99.2%, spectral efficiency of 37 bps/Hz, and throughput of 290 bits/Hz. Compared with existing models the proposed model achieves a less and a BER of 0.01. This proves that the proposed system performed well when compared to other existing techniques.

**Table 2.** Comparison of proposed models with existing methods

| Method | Accuracy (%) | BER | Spectral Efficiency (bps/Hz) | Throughput (bits/Hz) | Energy Efficiency (bits/J) |
|---|---|---|---|---|---|
| OMP | 79.0 | 0.19 | 30 | 165 | 1.6 |
| LMS | 80.0 | 0.20 | 34 | 185 | 2.0 |
| CNN | 98.7 | 0.15 | 33.8 | 275 | 6.3 |
| RNN (Proposed) | 99.2 | 0.01 | 37 | 290 | 7.5 |

### 4.5 Discussion

Unlike traditional Butler matrices that offer fixed beam directions, the proposed Recurrent Butler Forcing Attenuators Fourier Phase Distortionless Response Network introduces a dynamic adaptation mechanism through recurrent layers that learn and adjust beam directions over time. This is particularly effective in handling multipath fading, where temporal correlations in the channel state are exploited to stabilize the beamform. In contrast to zero-forcing methods, which suffer under imperfect CSI and cannot compensate for CTI, the modelled network uses an RNN-based structure with forcing attenuators to suppress interference by learning CTI signatures across time. The incorporation of Fourier Phase Distortionless Response **ensures** minimal phase error, leading to higher spectral efficiency compared to LMS and CNN-based beamformers. Additionally, the use of adaptive phase-shifting ensures real-time alignment of signal paths, maintains coherent beam output under mobility. The system also benefits from the phase tiniest variance control, which further sharpens the beam pattern by reducing unwanted side lobes. Overall, the network offers a scalable, interference-resilient solution tailored for ultra-dense mmWave environments.

## 5. CONCLUSION AND FUTURE WORK

Conclusively, the "Recurrent Butler Forcing Attenuators Fourier phase Distortionless Response Network" that has been presented for multi-user mmWave massive MIMO Systems offers a thorough resolution to the issue of existing systems. Initially, an Amalgam Butler Zero Forcing Matrix addresses multi-path fading and destructive interference by increasing signal combining efficiency and reducing ISI effects, resulting in improved system performance. Then, DAFT overcomes angular resolution changes across frequencies, resulting in consistent performance and scalability to a wide range of propagation settings.

Finally, the PTVSR significantly reduces CTI, improving beamforming accuracy despite the complications of coexisting wireless technologies. By incorporating these strategies into an RNN architecture, the system exhibits exceptional flexibility and resilience, opening the path for improved performance and reliability in complex propagation scenarios. At an SNR of 20dB, the model achieves a remarkable sum rate of 140 bits/s/Hz, high accuracy of 99.2%, spectral efficiency of 37 bps/Hz, throughput of 290 bits/Hz, and low BER of 0.01. This results in improved system performance reduced decoding errors, and enhanced adaptability to complex wireless environments. The proposed approach represents a significant advancement in the field of mmWave communication systems, offering a promising pathway toward overcoming the limitations posed by challenging propagation conditions and diverse wireless technologies.

### 5.1 Future scope

Future research will focus on reducing the computational overhead associated with the multi-layered RNN and hybrid modules by employing model compression techniques such as pruning, quantization, and knowledge distillation. Additionally, transitioning from MATLAB-based simulation to FPGA or GPU-accelerated environments will support real-time deployment. Further expansion of the model will target operation across wider mm Wave frequency bands (e.g., 30-100 GHz), with dynamic sub-band assignment mechanisms to handle spectrum fragmentation. The adaptation of the framework to support user mobility and rapid beam tracking will be investigated using lightweight attention mechanisms. Finally, field testing in hardware testbeds (e.g., 5G NR or WiGig platforms) will validate the real-world feasibility and robustness of the proposed system.

## REFERENCES


[1] Mchangama, A., Ayadi, J., Jiménez, V.P.G., Consoli, A. (2020). MmWave massive MIMO small cells for 5G and beyond mobile networks: An overview. In 2020 12th International Symposium on Communication Systems, Networks and Digital Signal Processing (CSNDSP), Porto, Portugal, pp. 1-6. https://doi.org/10.1109/CSNDSP49049.2020.9249602

[2] Rao, L., Pant, M., Malviya, L., Parmar, A., Charhate, S.V. (2021). 5G beamforming techniques for the coverage of intended directions in modern wireless communication: in-depth review. International Journal of Microwave and Wireless Technologies, 13(10): 1039-1062. https://doi.org/10.1017/S1759078720001622

[3] Albreem, M.A., Juntti, M., Shahabuddin, S. (2019). Massive MIMO detection techniques: A survey. IEEE Communications Surveys & Tutorials, 21(4): 3109-3132. https://doi.org/10.1109/COMST.2019.2935810

[4] Vaigandla, K.K., Venu, D.N. (2021). Survey on massive MIMO: Technology, challenges, opportunities and benefits. YMER, 20(11): 188-198. https://doi.org/10.37896/YMER20.11/25

[5] Liang, Y., Gao, N., Liu, T. (2020). Suppression method of inter-symbol interference in communication system based on mathematical chaos theory. Journal of King Saud University - Science, 32(2): 1749-1756. https://doi.org/10.1016/j.jksus.2020.01.012

[6] Jazea, N.A., Kadim, H.A., Sallomi, A.H. (2020). Study and analysis of intra-cell interference and inter-cell interference for 5G network. Journal of Engineering and Sustainable Development, 24(3): 43-57. https://doi.org/10.31272/jeasd.24.3.3

[7] Matthews, W., Ali, W., Ahmed, Z., Faulkner, G., Collins, S. (2021). Inter-symbol interference and silicon photomultiplier VLC receivers in ambient light. IEEE Photonics Technology Letters, 33(9): 449-452. https://doi.org/10.1109/LPT.2021.3067511

[8] Kaboutari, K., Abraray, A., Maslovski, S. (2024). Numerically optimized fourier transform-based beamforming accelerated by neural networks. Applied Sciences, 14(7): 2866. https://doi.org/10.3390/app14072866

[9] Li, H., Li, M., Liu, Q., Swindlehurst, A.L. (2020). Dynamic hybrid beamforming with low-resolution PSs for wideband mmWave MIMO-OFDM systems. IEEE Journal on Selected Areas in Communications, 38(9): 2168-2181. https://doi.org/10.1109/JSAC.2020.3007036

[10] Wang, W., Zhang, W., Wu, J. (2020). Optimal beam pattern design for hybrid beamforming in millimeter wave communications. IEEE Transactions on Vehicular Technology, 69(7): 7987-7991. https://doi.org/10.1109/TVT.2020.2992919

[11] Hong, S.H., Park, J., Kim, S.J., Choi, J. (2022). Hybrid beamforming for intelligent reflecting surface aided millimeter wave MIMO systems. IEEE Transactions on Wireless Communications, 21(9): 7343-7357. https://doi.org/10.1109/TWC.2022.3157880

[12] Mirzaei, J., ShahbazPanahi, S., Sohrabi, F., Adve, R. (2021). Hybrid analog and digital beamforming design for channel estimation in correlated massive MIMO systems. IEEE Transactions on Signal Processing, 69: 5784-5800. https://doi.org/10.48550/arXiv.2107.07622

[13] He, Y., Guo, X., Zheng, X., Yu, Z., Zhang, J., Jiang, H., Na, X., Zhang, J. (2022). Cross-technology communication for the internet of things: A survey. ACM Computing Surveys, 55(5): 1-29. https://doi.org/10.1145/3530049

[14] An, Z. (2021). On cross-technology Mutualism in the internet of things: Communication and localization. Polyu Electronic Theses. https://theses.lib.polyu.edu.hk/handle/200/11784.

[15] Zheng, X.L., Xia, D., Guo, X.Z., Liu, L., He, Y., Ma, H.D. (2020). Portal: Transparent cross-technology opportunistic forwarding for low-power wireless networks. In Proceedings of the Twenty-First International Symposium on Theory, Algorithmic Foundations, and Protocol Design for Mobile Networks and Mobile Computing, New York, United States, pp. 241-250. https://doi.org/10.1145/3397166.3409134

[16] Carrera, D.F., Vargas Rosales, C., Villalpando Hernandez, R., Galaviz Aguilar, J.A. (2020). Performance improvement for multi user millimeter wave massive MIMO systems. IEEE Access, 8: 87735-87748. https://doi.org/10.1007/s11277-023-10660-5

[17] Dilli, R. (2021). Performance analysis of multi user massive MIMO hybrid beamforming systems at millimeter wave frequency bands. Wireless Networks, 27(3): 1925-1939. https://doi.org/10.1007/s11276-021-02546-w

[18] Zhang, Y., Du, J., Chen, Y., Li, X., Rabie, K.M., Kharel, R. (2020). Dual iterative hybrid beamforming design for millimeter wave massive multi user MIMO systems with sub connected structure. IEEE Transactions on Vehicular Technology, 69(11): 13482-13496. https://doi.org/10.1109/TVT.2020.3029080

[19] Huang, S., Ye, Y., Xiao, M. (2020). Hybrid beamforming for millimeter wave multi user MIMO systems using learning machine. IEEE Wireless Communications Letters, 9(11): 1914-1918. https://doi.org/10.1109/LWC.2020.3007990

[20] Zhang, Y., Du, J., Chen, Y., Li, X., Rabie, K.M., Kharel, R. (2020). Near optimal design for hybrid beamforming in mmWave massive multi user MIMO systems. IEEE Access, 8: 129153-129168. https://doi.org/10.1109/ACCESS.2020.3009238

[21] Zhang, Y., Du, J., Chen, Y., Han, M., Li, X. (2019). Optimal hybrid beamforming design for millimeter wave massive multi user MIMO relay systems. IEEE Access, 7: 157212-157225 https://doi.org/10.1109/ACCESS.2019.2944203

[22] Lizarraga, E.M., Maggio, G.N., Dowhuszko, A.A. (2021). Deep reinforcement learning for hybrid beamforming in multi user millimeter wave wireless systems. In 2021 IEEE 93rd Vehicular Technology Conference (VTC2021 Spring), Helsinki, Finland, pp. 1-5. https://doi.org/10.1109/VTC2021-Spring51267.2021.9449053

[23] Jafri, M., Anand, A., Srivastava, S., Jagannatham, A.K., Hanzo, L. (2022). Robust distributed hybrid beamforming in coordinated multi user multi cell mmWave MIMO systems relying on imperfect CSI. IEEE Transactions on Communications, 70(12): 8123-8137. https://doi.org/10.1109/TCOMM.2022.3189237

[24] Zhan, J., Dong, X. (2021). Interference cancellation aided hybrid beamforming for mmWave multi user massive MIMO systems. IEEE Transactions on Vehicular Technology, 70(3): 2322-2336. https://doi.org/10.1109/TVT.2021.3056297

[25] Muthukumaran, N. (2023). Optimized CNN and adaptive RBFNN for channel estimation and hybrid precoding approaches for multi user millimeter wave massive MIMO. International Journal of Electronics, 112(7): 1295-1318. https://doi.org/10.1080/00207217.2024.2372060